International Journal of Concrete Structures and Materials

RESEARCH

Open Access

Transport Characteristics and Corrosion Behavior of Ultra-High Performance Fiber-Reinforced Concrete with the Key Mix Parameters

Shamsad Ahmad[1,2], Ashraf A. Bahraq[2*], Amin Al-Fakih[1,2*], Moruf Olalekan Yusuf[3] and Mohammed A. Al-Osta[1,2]

Abstract

The presence of low-quality coarse aggregates and exposure to aggressive conditions are the two major problems with the durability of concrete. Therefore, an alternative concrete with enhanced properties to prevent fluid and ionic mobility compared to conventional concrete is needed. This study investigated the effects of main mix parameters on the transport characteristics and corrosion behavior of ultra-high performance fiber-reinforced concrete (UHPFRC). A set of 27 UHPFRC mixtures with different combinations of w/b ratio, cement, and silica fume contents, based on a 3^3-factorial experiment design, were prepared and tested for water permeability, chloride penetrability, electrical resistivity, chloride profile, and corrosion current density. The results showed that UHPFRC mixtures exhibited excellent durability properties characterized by negligible water penetration (< 15 mm), negligible and very low chloride permeability when the w/b ratio was 0.15 (< 100 Coulombs) and up to 0.2 (< 300 Coulombs), respectively, and very low chloride concentrations at the rebar level (0.03–0.18 wt.%). All resistivity values were within the range of 26.7–78.8 kΩ cm (> 20 kΩ cm) and pH values were 12.41–13.01, indicating the implausible likelihood of corrosion in the UHPFRC mixtures. This was confirmed through the corrosion current density measurements of reinforced UHPFRC specimens after 450 days of chloride exposure, which were below the critical limit for the corrosion initiation of reinforcing steel. Finally, the experimental data were statistically analyzed and fitted for all the listed tests, and models were developed for them using the regression analysis such that regression coefficients were within 0.90–0.99.

Keywords Ultra-high performance concrete, UHPC, Permeability, Chloride-induced corrosion, Chloride model, Durability

Journal information: ISSN 1976-0485 / eISSN 2234-1315.

*Correspondence:
Ashraf A. Bahraq
ashraf.bahraq@kfupm.edu.sa
Amin Al-Fakih
aminali.fakih@kfupm.edu.sa
Full list of author information is available at the end of the article

1 Introduction

Producing highly durable transport concrete poses significant challenges. Specifically, in regions like Saudi Arabia, where low-quality coarse aggregates and harsh weather conditions prevail, making concrete durability even more critical. Consequently, there is a pressing need to explore alternative concretes with superior durability properties, particularly in hindering fluid and ionic migration inside concrete compared to traditional ones. A less-permeable concrete matrix can effectively prevent the ingress of aggressive chemicals such as chloride or sulfate ions, thus protecting reinforced concrete structures from degradation (Bajaber & Hakeem, 2021; Tayeh et al., 2019; Zhao et al., 2022). Among the identified alternatives, ultra-high performance fiber-reinforced concrete (UHPFRC) stands out. This advanced material has optimized particle packing of fine and ultrafine powders, complemented by the inclusion of steel fibers (Abdellatief et al., 2023; Soliman & Tagnit-Hamou, 2017; Yoo & Yoon, 2016). It has been reported that UHPFRC possesses excellent mechanical properties, including compressive strength (> 150 MPa), tensile strength (> 15 MPa), and high ductility (Ahmad et al., 2024; Amran et al., 2022; Bahraq et al., 2019; Osta et al., 2020).

The high content of the reactive powders and low water-to-binders ratio (w/b < 0.2) have resulted in ultra-high strength and durability characteristics (Richard & Cheyrezy, 1994, 1995; Shi et al., 2015). Generally, ordinary Portland cement (OPC) and silica fume (SF) are utilized as reactive binders in the production of UHPFRC mixtures (Amran et al., 2022; Wang et al., 2023). This results in improving the particle packing density of UHPFRC (Du et al., 2021). In addition, the dense and uniform microstructure of its matrix was reported, which is attributed to several factors, including the close particle packing and pozzolanic reactions (Shi et al., 2015; Wen et al., 2022). Tam et al. (2012) examined the water permeability of UHPFRC at varying w/b ratios and superplasticizer quantities. Their findings indicated that microstructural density and void discontinuity led to lower water permeability in UHPFRC compared to conventional concrete. The strength-permeability relationship showed that the water permeability of UHPFRC decreased with an increase in compressive strength. Toledo et al. (2012) found that the concrete structure of UHPFRC was dense and exhibited no permeability or porosity. All these aspects have together resulted in an impermeable matrix of UHPFRC mixtures (Du et al., 2021), which is a fundamental property of the transport characteristics of concrete (Ahmad et al., 2023; Wang et al., 2021).

Li et al. (2020) conducted a review on the durability properties of UHPFRC mixtures, emphasizing their notably low penetration of water and chemical species, which presents exceptional resistance to carbonation and reinforcement corrosion. Roux et al. (1996) studied the transport properties and corrosion propagation and found no pores exceeding a diameter of 15 nm in UHPFRC mixtures. Unlike the low-cement concrete with 30 MPa compressive strength and grade 80 MPa high-performance concrete (HPC), the UHPFRC exhibited superior granular compactness, resulting in a compressive strength above 100 MPa, very high resistivity, minimal water absorption and chloride ion permeability, and exhibited no carbonation due to reduced porosity resulting from its low water content. The chloride penetrability of UHPFRC was investigated by Graybeal and Hartmann (Graybeal & Hartmann, 2003), who reported rapid chloride ion penetration as low as 10 Coulombs under various curing conditions. El-Dieb (2009) investigated UHPFRC mixtures incorporating OPC and SF, observing that the inclusion of steel fibers impacted the electrical resistivity and microstructure density, mitigating the intrusion of chloride and sulfate ions. However, they noted that the influence of fiber content was less significant compared to the w/b ratio and mineral admixtures. Furthermore, Wen et al. (2022) highlighted the positive impact of steel fibers on enhancing the durability of UHPFRC, particularly in terms of resistance to chloride permeability and shrinkage. A study by Abbas et al. (2015) concluded that the presence of steel fibers contributes to mitigating chloride permeability compared to fiber-free mixtures. The dense microstructure of UHPFRC mixtures significantly contributes to impeding chloride ion ingress, moisture, and oxygen, which are essential elements for corrosion onset. This assertion finds validation through SEM, EDS, and MIP experiments, illustrating enhanced durability via crack formation and growth restriction, reduced penetrability, and porosity. Moreover, an examination at a depth of 3 mm from the specimen surface revealed limited corrosion of fibers confined to the surface (up to 1 mm). A similar observation was also reported by Lv et al. (2021).

This study addresses a significant gap in the literature by thoroughly investigating the transport properties and corrosion behavior of UHPFRC, which have received comparatively less attention than its mechanical properties. A detailed experimental program is designed, involving preparing and testing a total of 27 UHPFRC mixtures with varied combinations of w/b ratio, cement, and silica fume contents. A series of tests were conducted, including water permeability, chloride penetrability, electrical resistivity, and corrosion current density. Subsequently, the results were statistically analyzed to develop empirical models to establish the relationships between fundamental transport properties and the key mixture parameters. By examining the durability characteristics of UHPFRC mixtures and elucidating the

models governing transport properties and corrosion performance in relation to key mixture parameters, this research provides valuable insights that could substantially advance the understanding of the material's behavior under aggressive environmental conditions and the application of UHPFRC in various structural contexts. Hence, UHPFRC holds promise for advancing sustainable infrastructure development through improving the durability characteristics and, therefore, the lifespan of structures beyond their mechanical attributes.

2 Experimental Program

2.1 Materials

Type I ordinary Portland cement (OPC) complying with ASTM C150 (ASTM International, 2019b) was utilized in the present work. The 7- and 28-day compressive strengths of OPC were 29.97 and 37.76 MPa, respectively, (ASTM C150 specifies the minimum corresponding values of 19 and 28 MPa). Silica fume (SF), having very fine vitreous particles, was also used. The chemical compositions of the binders used are shown in Table 1. Fine dune quartz sand, which is abundantly and locally available in the deserts of Saudi Arabia, was used as the sole aggregate with natural grading (150 to 600 µm in size), as shown in Fig. 1. Dune sand possesses desired properties, including water absorption of 0.4%, a specific gravity of 2.53, rounded grains, and a smooth surface texture.

A chloride-free ASTM C494 (ASTM International, 2017) compliant polycarboxylic ether (PCE) Glenium 51 superplasticizer (SP) with a specific gravity and water content of 1.095 and 65 wt.%, respectively, was added to the mixtures to gain the wanted flow (Ahmad et al., 2015). The volume of the superplasticizer is varied to achieve a flow within 200 ± 20 mm. Micro-copper steel fibers that complied with ASTM A820 (ASTM International, 2021) were used in the UHPFRC mixtures. The steel fiber has a length and diameter of 13 mm and 0.22 mm, respectively, such that the aspect ratio (length/diameter) is 59. The tensile strength of the steel is approximately 2850 MPa. Fig. 2a displays the steel fiber.

2.2 Design of Experiment

In the current study, three key factors affecting the UHPFRC mixtures were investigated. These included the w/b ratio (0.15, 0.175, and 0.20), OPC content (1000, 1100, and 1200 kg/m^3), and SF dosage (15, 20, and 25% of cement). Thus, the factors were considered with three levels as per 3^3-factorial experimental design, i.e., 27 UHPFRC mixtures were made. The mix proportions of these mixtures are presented in Table 2.

Table 1 Chemical composition of OPC and SF

Material	Oxides composition (wt.%)								LOI*	Specific gravity
	SiO_2	Al_2O_3	Fe_2O_3	CaO	MgO	SO_3	Na_2O	K_2O		
OPC	22	5.64	3.8	64.35	2.11	2.1	0.19	0.36	0.7	3.15
SF	86.75	0.41	2.12	0.41	0.18	0.77	0.17	0.67	3.35	2.25

* Loss on ignition

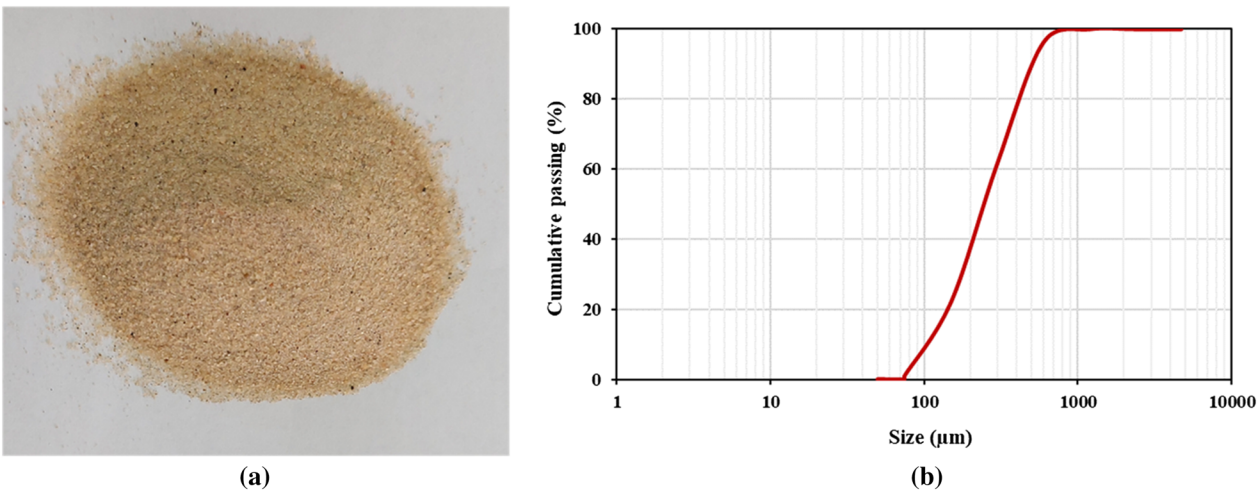

Fig. 1 **a** Dune sand; **b** Particle size distribution of dune sand

(a) **(b)**

Fig. 2 **a** Micro copper coated steel fibres; and **b** Planetary mixer

Table 2 Proportion of UHPFRC mixtures

Mix No	Investigated mix parameters			Mix proportion by volume					
	w/b	OPC (kg/m^3)	SF (%)	OPC	SF	Water	Fiber	SP	Sand
UHPFRC-1	0.15	1000	15	0.32	0.07	0.17	0.02	0.04	0.39
UHPFRC-2	0.15	1000	20	0.32	0.09	0.18	0.02	0.04	0.35
UHPFRC-3	0.15	1000	25	0.32	0.11	0.19	0.02	0.04	0.32
UHPFRC-4	0.15	1100	15	0.35	0.07	0.19	0.02	0.04	0.33
UHPFRC-5	0.15	1100	20	0.35	0.10	0.20	0.02	0.04	0.29
UHPFRC-6	0.15	1100	25	0.35	0.12	0.21	0.02	0.04	0.26
UHPFRC-7	0.15	1200	15	0.38	0.08	0.21	0.02	0.04	0.27
UHPFRC-8	0.15	1200	20	0.38	0.11	0.22	0.02	0.05	0.23
UHPFRC-9	0.15	1200	25	0.38	0.13	0.23	0.02	0.05	0.19
UHPFRC-10	0.175	1000	15	0.32	0.07	0.20	0.02	0.02	0.37
UHPFRC-11	0.175	1000	20	0.32	0.09	0.21	0.02	0.02	0.34
UHPFRC-12	0.175	1000	25	0.32	0.11	0.22	0.02	0.02	0.31
UHPFRC-13	0.175	1100	15	0.35	0.07	0.22	0.02	0.02	0.32
UHPFRC-14	0.175	1100	20	0.35	0.10	0.23	0.02	0.02	0.28
UHPFRC-15	0.175	1100	25	0.35	0.12	0.24	0.02	0.02	0.25
UHPFRC-16	0.175	1200	15	0.38	0.08	0.24	0.02	0.02	0.26
UHPFRC-17	0.175	1200	20	0.38	0.11	0.25	0.02	0.02	0.22
UHPFRC-18	0.175	1200	25	0.38	0.13	0.26	0.02	0.02	0.18
UHPFRC-19	0.2	1000	15	0.32	0.07	0.23	0.02	0.02	0.35
UHPFRC-20	0.2	1000	20	0.32	0.09	0.24	0.02	0.02	0.32
UHPFRC-21	0.2	1000	25	0.32	0.11	0.25	0.02	0.02	0.28
UHPFRC-22	0.2	1100	15	0.35	0.07	0.25	0.02	0.01	0.29
UHPFRC-23	0.2	1100	20	0.35	0.10	0.26	0.02	0.01	0.26
UHPFRC-24	0.2	1100	25	0.35	0.12	0.28	0.02	0.01	0.22
UHPFRC-25	0.2	1200	15	0.38	0.08	0.28	0.02	0.01	0.23
UHPFRC-26	0.2	1200	20	0.38	0.11	0.29	0.02	0.01	0.19
UHPFRC-27	0.2	1200	25	0.38	0.13	0.30	0.02	0.01	0.15

The steel fiber content was kept constant at 2% by volume in all the mixtures.

2.3 Preparation and Curing of Mixtures

The UHPFRC mixtures were prepared through a casting procedure obtained from previously published works (Ahmad et al., 2014, 2016; Bahraq et al., 2019) and also from acquired laboratory experience. Initially, the dry powders of the OPC, SF, and sand were placed into the planetary mixer rotating for 3 min. The liquid solution was prepared by mixing the SP with water, which was then added in half quantity to the mixer and allowed to be thoroughly mixed with the materials for 3 min. Subsequently, the remaining half was then added and mixed for an additional 10 min, followed by the slow dispersal of the steel fibers for 2 min. The total mixture was further mixed for 3 min to ensure uniformity and homogeneity. It took about 20–25 min to complete the mixing process, as mixing the UHPFRC requires uniform consistency. The concrete that had been cast into the moulds was then vibrated until it had completely consolidated. To minimize moisture loss, the specimens were covered with a plastic sheet for 24 h after casting and placed in the laboratory environment at an ambient temperature of about 22 °C. The specimens were demoulded in the next day and kept in a curing tank until testing day.

After completing the mixing, the UHPFRC mixes were tested for consistency in accordance with the procedure of ASTM C1437 (ASTM International, 2015) by recording the average diameter that follows the dropping of the mixture placed in the mini slump cone flow table from 12.5 mm height with 25 strokes in 15 s. The measured flow diameter of the mixes was in the range of 180–220 mm. The compressive and flexural tensile strengths were determined by testing 50-mm cube and 40×40×160 mm prism specimens, respectively. The average 28-day values of the compressive strength and flexural tensile strength were in the range of 128–135 MPa and 27–32 MPa, respectively. Further information on the mechanical properties of UHPFRC mixtures can be found in the work reported by Ahmad et al. (2015).

2.4 Transport Properties Testing

The UHPFRC specimens were prepared and subjected to a series of tests, including water permeability, chloride penetrability, electrical resistivity, and corrosion current density. The average of the test results of three replicate specimens from each mixture for each specific test was considered for the analysis.

2.4.1 Water Permeability

The water permeability test was conducted according to DIN 1048 (German Institute for Standardization, 1991). Cubical concrete specimens with a size of 100-mm were used in this test after 28 days of curing, as depicted in Fig. 3a. The specimens were first air-dried for 24 h before being oven-dried for 72 h at 70 °C. They were then air-cooled for 24 h under standard laboratory conditions. Water was applied to one face of the specimen for 72 h at 5 bar pressure, then split open to measure the water penetration depth.

2.4.2 Rapid Chloride Permeability

After 28 days of water curing, the chloride ion penetrability was measured according to ASTM C1202 (ASTM International, 2019a) and AASHTO T-277 (AASHTO, 1989). The test setup for rapid chloride permeability is depicted in Fig. 3b. A side epoxy-coated disk 50-mm thick was cut from the center of the cylindrical specimen (75×150 mm), and the disc was then saturated in water for 24 h. Direct current (DC) of 60 V monitored every 30 min for 6 h was kept across two cells: 3% NaCl cathode (upstream) and 0.3 M NaOH (downstream) filled cells. The total charge passed through the specimen was recorded.

2.4.3 Electrical Resistivity

Cylindrical specimens (75×150 mm) with centrally embedded reinforcing steel were used in the electrical resistivity test, as shown in Fig. 3c. The specimens were cured for 28 days and then subjected to a chloride solution (5% NaCl) for 450 days. Then, they were prepared for testing by making 50 mm-spaced, two 8 mm-deep holes filled with conductive gel using a 6 mm drill. The electrical resistivity was then measured using a two-probe Wenner method (Dehghanpour & Yilmaz, 2020).

2.4.4 Chloride Concentration

A week after 28 days of water curing, the dry specimens were prepared to determine the chloride concentration. The specimens were completely coated, leaving out the top surface. The prepared specimens were immersed in a chloride solution (5% NaCl) for a period of six months with the uncoated surface faced down. The specimens were cleaned, dried, and then sliced at depths of 0–5, 10–15, 20–25, 30–35, and 40–45 mm, as displayed in Fig. 3d, starting from the uncoated surface. The epoxy on the sliced samples was removed, and the samples were distinctively powdered and sieved through an ASTM #100 sieve. The powdered samples (3 g) were dissolved in 3 ml of HNO_3 acid and 47 ml of distilled water, shaken rigorously, and kept for 24 h. The filtrate was then diluted

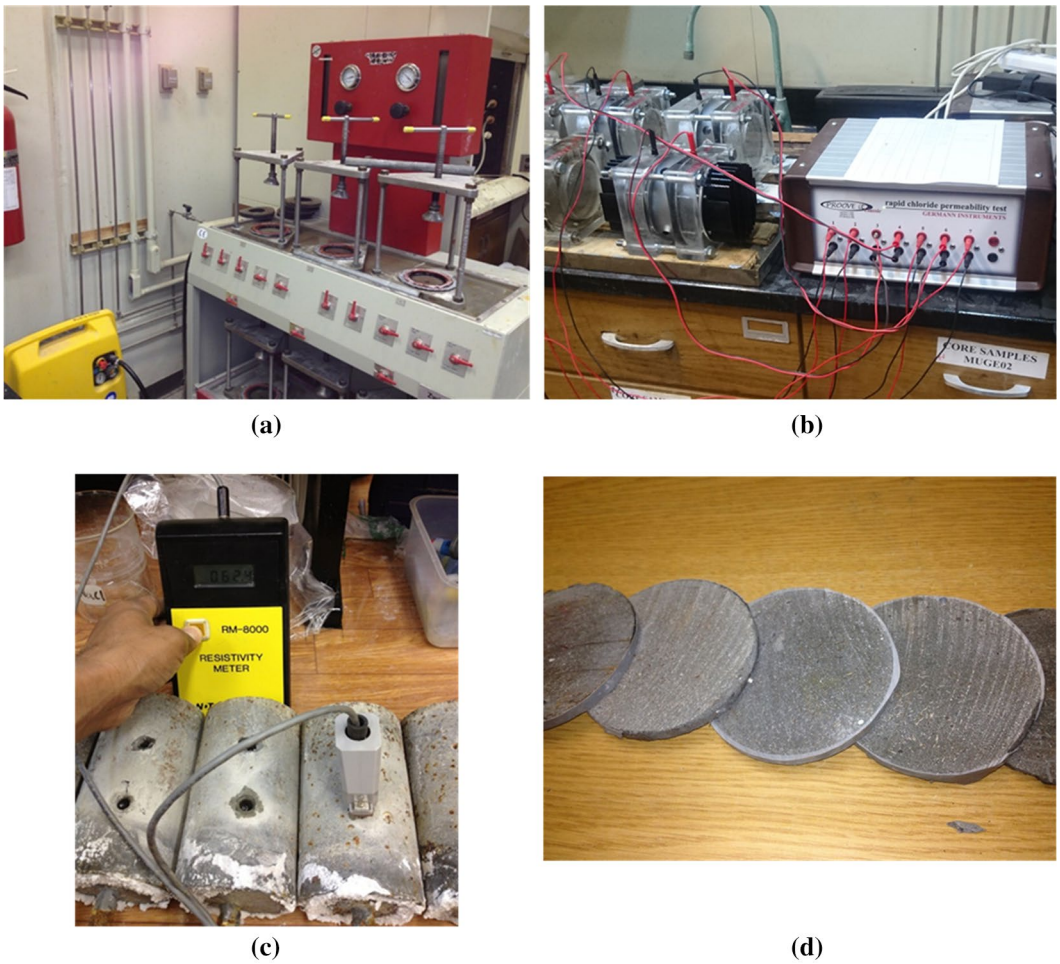

Fig. 3 Transport properties testing: **a** water permeability; **b** rapid chloride permeability; **c** electrical resistivity; and **d** slices for chloride concentration

with distilled water to make 100 ml of solution. The chloride concentrations at the surface (C_S at $x=0$) and rebar level (C_r at $x=25$ mm) were determined.

2.5 Reinforcement Corrosion

The corrosion current density (I_{corr}) of the UHPFRC mixtures was measured to evaluate the reinforcement corrosion. UHPFRC cylinders with embedded steel rebar were prepared for corrosion experiment after water curing of 28 days. The UHPFRC specimens were exposed to a 5% NaCl solution for a period of 450 days, and the I_{corr} was recorded every 30 days intervals. Fig. 4 shows the adopted methodology for evaluating the I_{corr} of the mixtures. The linear polarization resistance (LPR) (Stern & Geary, 1957) was used as an electrochemical method to measure the I_{corr} of the specimens. The steel rebar and stainless-steel plate were employed as working and counter electrodes, respectively, while the saturated calomel electrode (SCE) was utilized as a reference electrode. The three electrodes were connected to a Potentiostat/Galvanostat (ACM equipment). A polarization scan of ± 10 mV was set at a rate of 0.1 mV/s. Using the polarization resistance (Rp), I_{corr} was obtained through the Stern and Geary formula (Stern & Geary, 1957), as expressed in Eq. (1). The constant B can be obtained using the anodic and cathodic Tafel constants (β_a and β_c), as shown in Eq. (2). However, in the lack of data on Tafel constants, a value of 120 mV can be used for steel in a highly resistant medium, i.e., $B=26$ mV (Lambert et al., 1991). After the completion of the exposure period, the cylindrical reinforced concrete specimens were split to expose the steel for the visual inspection examination.

$$I_{corr} = B/R_P \tag{1}$$

$$B = \frac{(\beta_a * \beta_c)}{2.3(\beta_a + \beta_c)} \tag{2}$$

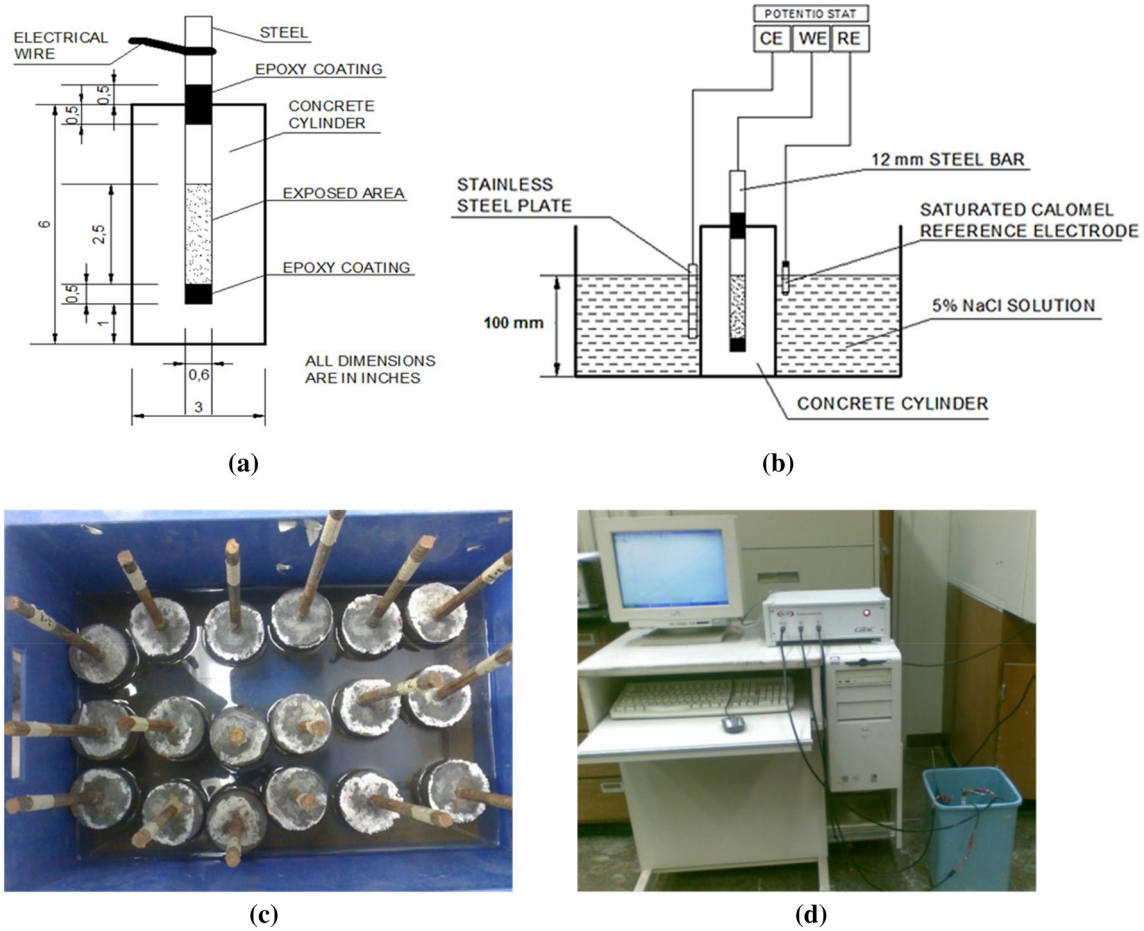

Fig. 4 Corrosion testing setup: **a** reinforced concrete cylinder; **b** schematic representation of the testing setup; **c** specimen under solution exposure; and **d** Corrosion current density measurements

3 Results and Discussion

3.1 Water Penetration Depths

Fig. 5 shows the water penetration depth with the w/b variations of all UHPFRC mixtures after 28 days of water curing. The results indicated that the penetration depths of the mixtures decreased with the decrease in w/b ratios. The use of a high w/b ratio initially contributes to the hydration process of cementitious materials; however, the presence of non-reactive water due to the high w/b ratio is possible as the UHPFRC mixture is a dense composite, packed with very fine materials. Thus, the availability of free water, referring to water that does not participate in the hydration reaction of cement, leads to the formation of the interconnected pores within the UHPFRC matrix. These pores can provide pathways for water and other substances to penetrate the concrete. Specifically, increasing the w/b ratio from 0.15 to 0.175 at a constant OPC content of 1000 kg/m^3 could cause an increase in the penetration depth by around 29%, while increasing the OPC content to 1100 kg/m^3 with SF maintained at 15% caused a reduction by 19%. The reduction was further reduced to 43% as the SF increased to 25%. At low w/b ratios (0.15 and 0.175), the use of a high quantity of cement content beyond 1100 kg/m^3 is not always diminishing the permeability of the concrete. This is due to the fact that increasing the cement beyond the optimum required for the hydration reaction does not influence pore blockage. However, at a higher w/b ratio (0.2), the presence of a high cement proportion results in a consistent reduction in the concrete permeability, as shown in Fig. 5. In addition, the results reveal that the introduction of a higher quantity of SF (25%) appears to be beneficial to concrete permeability reduction. At the optimum SF and cement, all hydrations could have taken place while SF had a threshold for the consumption of portlandite present in the matrix. This assertion is supported by the

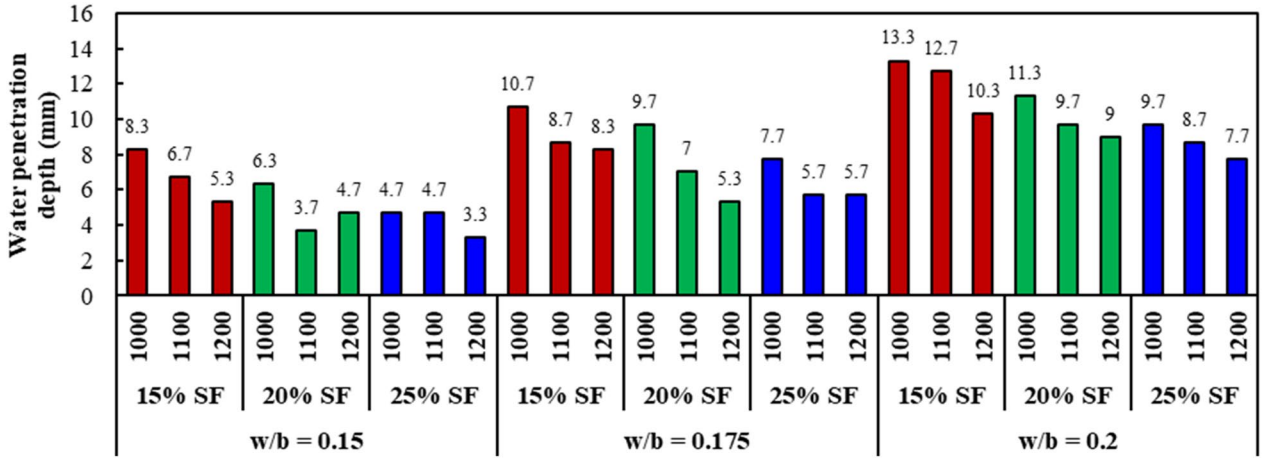

Fig. 5 Water penetration depth for different w/b ratios, OPC and SF contents

recorded water penetration depth of 9.7 mm for a w/b of 0.2 as SF increased from 20 to 25% (Fig. 5). It can be noted that all the UHPFRCs can be classified as "low permeable mixtures" since their penetration depths were far lower than the 30 mm threshold for low permeability.

3.2 Chloride Penetrability

Fig. 6 shows the values of the charge passed in all the UHPFRC mixtures measured after 28 days of water curing. As observed from Fig. 6, the chloride penetration decreased as the w/b ratio decrease and the OPC and SF dosages increased. The lowest charge passed (20 Coulombs) was found in the mixture prepared with the highest contents of OPC (1200 kg/m^3) and SF (25%), while the highest value (242 Coulombs) was registered in the mixture with the lowest binders (1000 kg/m^3 OPC and 15% SF). The response of chloride permeability to OPC content appears to be linear graphically, as shown in Fig. 6. Increasing cement content from 1000 to 1200 kg/m^3 at a lower w/b ratio (0.15) could reduce the chloride permeability by 74%. At a w/b ratio of 0.2, the reduction could be 63% if the SF increased from 15 to 25% but reduced to 13% if the SF is maintained at 20%. The contribution of higher OPC content is more evident at a higher w/b ratio (0.2) compared to 0.15. The SF consistently reduced the chloride permeability at all levels of the w/b ratio.

According to ASTM C1202 (ASTM International, 2019a) and related literature (Broomfield, 2003), the chloride ion penetrability can be classified based on the charge passed in Coulombs: high (> 4000), moderate (2000–4000), low (1000–2000), very low (100–1000), and negligible (< 100). In the current study, all the UHPFRCs prepared with a w/b ratio of 0.15 showed chloride permeability lower than 100 Coulomb, indicating their negligible chloride ion penetrability, while

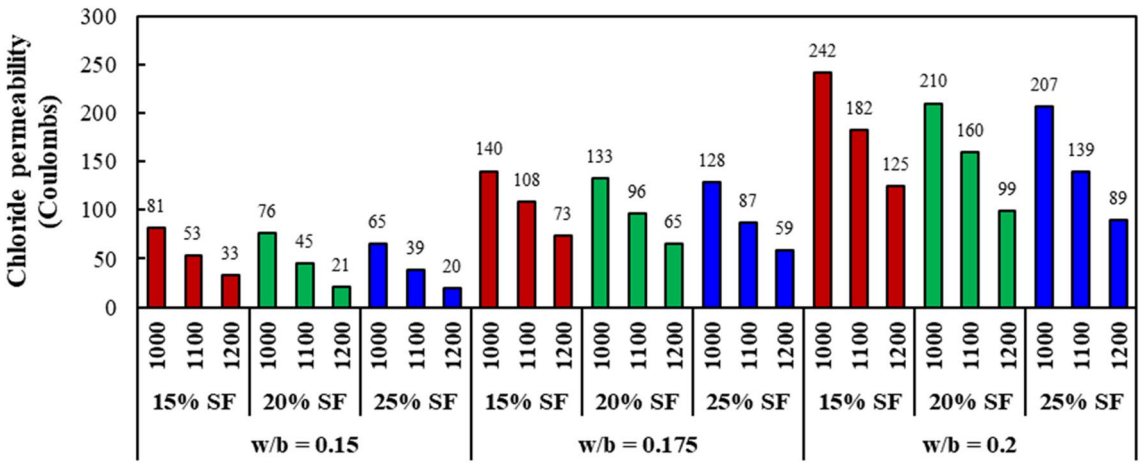

Fig. 6 Chloride permeability for various UHPFRC mixtures

other mixtures were in the category of low chloride permeability.

3.3 Electrical Resistivity

The electrical resistivity measurements of all UHPFRC mixtures are given in Fig. 7. From the data presented in this figure, it is evident that resistivity increased with concrete self-desiccation, which increased as the w/b ratio decreased. It can be said that the impact of self-desiccation to generate denser microstructure through secondary hydration is more reflexive at the w/b ratio of 0.15 compared to when it increases to 0.175 and 0.2 (Fig. 7). Previous studies also confirmed the dense microstructure of the UHPFRC mixtures through microstructural examinations, including SEM and EDS analyses (Chen et al., 2019; Dong et al., 2022; Zhao et al., 2023). The formation of pores is expected to be higher in the concrete with a higher w/b ratio, thereby lowering and increasing its resistivity and conductivity, respectively. In other words, as the w/b ratio increases, the resistivity decreases while the porosity within the concrete matrix and the propensity for chloride migration increase. Besides, it was noted that the electrical resistivity increased as the contents of OPC and SF increased. At the SF level of 25%, it appears to contribute to resistivity and more significantly at the w/b ratios of 0.175 and 0.2%. At SF content of 25%, increasing cement content from 1000 to 1100 and 1200 kg/m^3 increased the resistivity by 14.3, 32.7, and 36.6% for corresponding w/b ratios of 0.15, 0.175, and 0.2. Compared to the electrical resistivity thresholds for depassivated steel (Broomfield, 2003; Bungey & Grantham, 2006), all the UHPFRC mixtures showed a negligible tendency for the likelihood of corrosion due to higher resistivity than 20 kΩ cm.

3.4 Chloride Profile

In terms of chloride concentrations (C_x) given as % by weight of cement versus the depth, the chloride profiles of all mixtures are shown in Fig. 8. The results indicated a typical chloride profile of all mixtures, where the chloride concentrations were found to be decreasing with depth. Generally, the UHPFRC with a w/b of 0.2 had the highest chloride concentrations, while those with a lower w/b ratio (0.15) registered the least chloride concentrations.

To analyze the impacts of the key mix parameters on chloride ingress, the chloride concentrations at the surface (C_s) and at the rebar level (C_r assumed at 25 mm) were studied, as shown in Fig. 9. The concentrations at the surface and rebar position were found to be in the range of 0.293–0.53 and 0.03–0.18 wt.%, respectively. This indicated that the UHPFRC mixtures effectively contributed to suppressing the ingress of the Cl^- ions, as evidenced by reducing the concentrations at the rebar level by 80% on average. As shown in Fig. 9, it can be observed that the mixtures with a higher w/b ratio (0.2) and lower OPC content (1000 kg/m^3) registered the highest C_r of around 0.18 wt.%, while the mixtures with a lower w/b (0.15) and a relatively higher OPC dosage (1100 kg/m^3) exhibited the lowest values (0.03 wt.%). This indicated that the concrete's surficial density and too high cement content contributed to the surficial density. However, it can be seen that the OPC content of 1100 kg/m^3 outperformed that of 1200 kg/m^3 at a lower w/b ratio (0.2), implying that the excess cement content beyond what is required for hydration and strength development may not prevent chloride ions' ingression. Moreover, the admixing of higher amounts of SF resulted in a consistent decrease in the chloride concentration. For example, the mixtures with 1000 kg/m^3 and admixed with 25% SF yielded a decrease in the chloride concentration of around 48% compared to those having 15% SF. This can

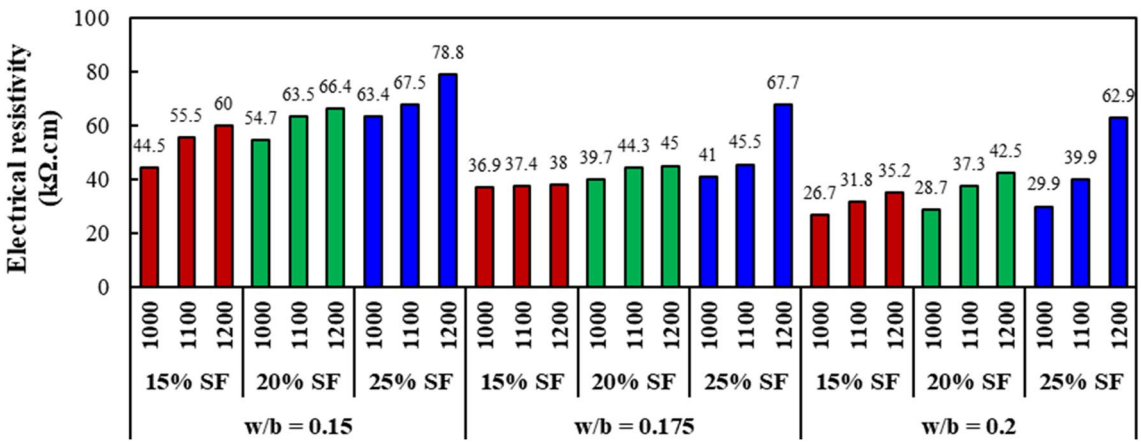

Fig. 7 Electrical resistivity for different UHPFRC mixtures

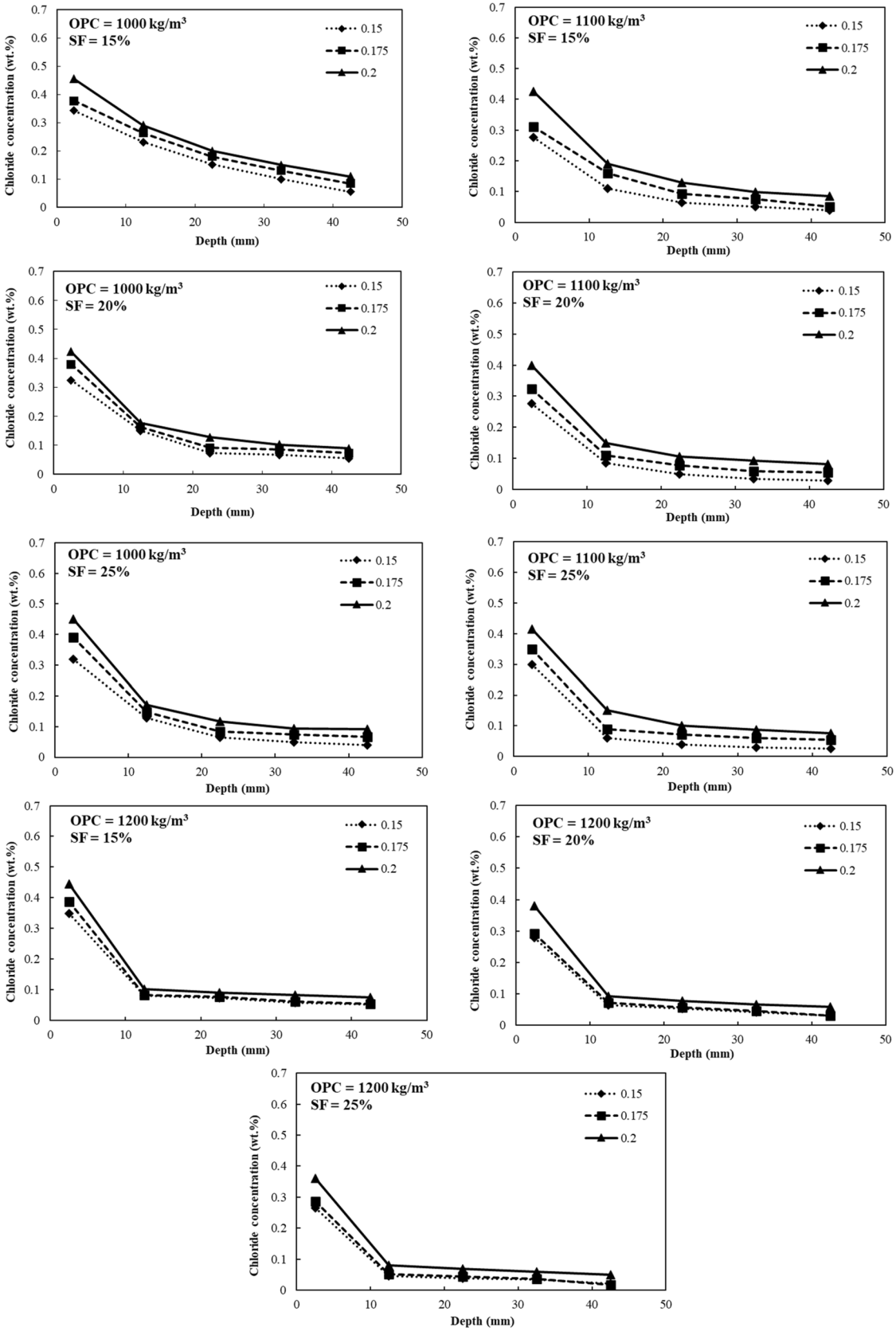

Fig. 8 Chloride profiles of different mixtures (expressed as wt.% of cement content)

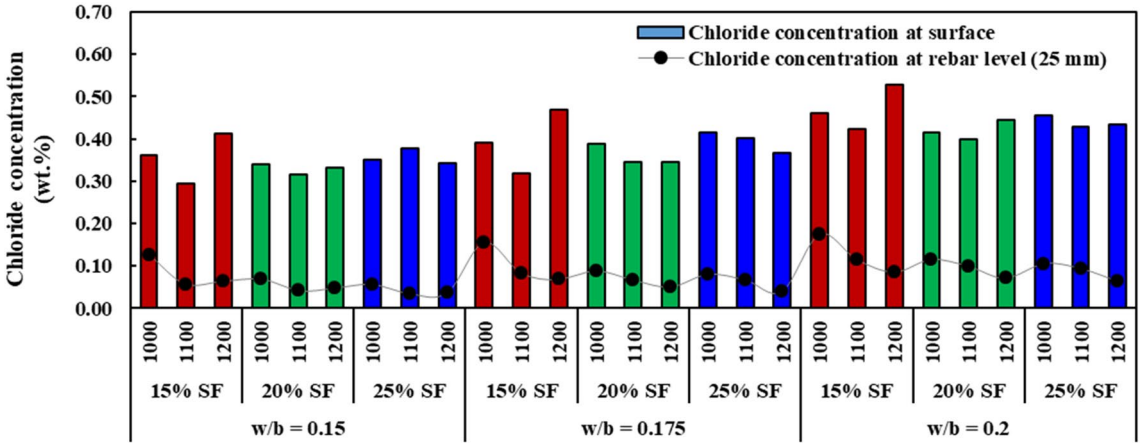

Fig. 9 Chloride concentration, expressed as %wt. of cement, for different w/b ratios, OPC and SF contents

be attributed to the finer nature of SF, which plays a role in the blockage of transport channels and also reflects its impact on the reduction of chloride migration (Saleh et al., 2023).

Using the obtained experimental data, a regression model was also developed for predicting the chloride profile of UHPFRC mixtures, as shown in Fig. 10. A simple power-curve model was established to fit the data, which showed an excellent regression coefficient (R^2) of 0.99. Equation (3) expresses the relation between the chloride concentration (Y, wt.%) and the depth (X, mm). As shown in Fig. 10, the chloride concentration at the depth of rebar in all mixtures is not up to the chloride threshold level (CTL) of 0.3–0.5 wt.% of cement, which could cause corrosion initiation in reinforced concrete structures (Angst et al., 2009). Theoretically, if the chloride concentration at the reinforcing rebar, i.e., at concrete cover depth, is not exceeding the CTL, a passive state will occur (Ahmad, 2003). This hypothesis was confirmed through the corrosion current density measurements, as discussed in the subsequent section.

$$Y = 0.7X^{-0.7} \tag{3}$$

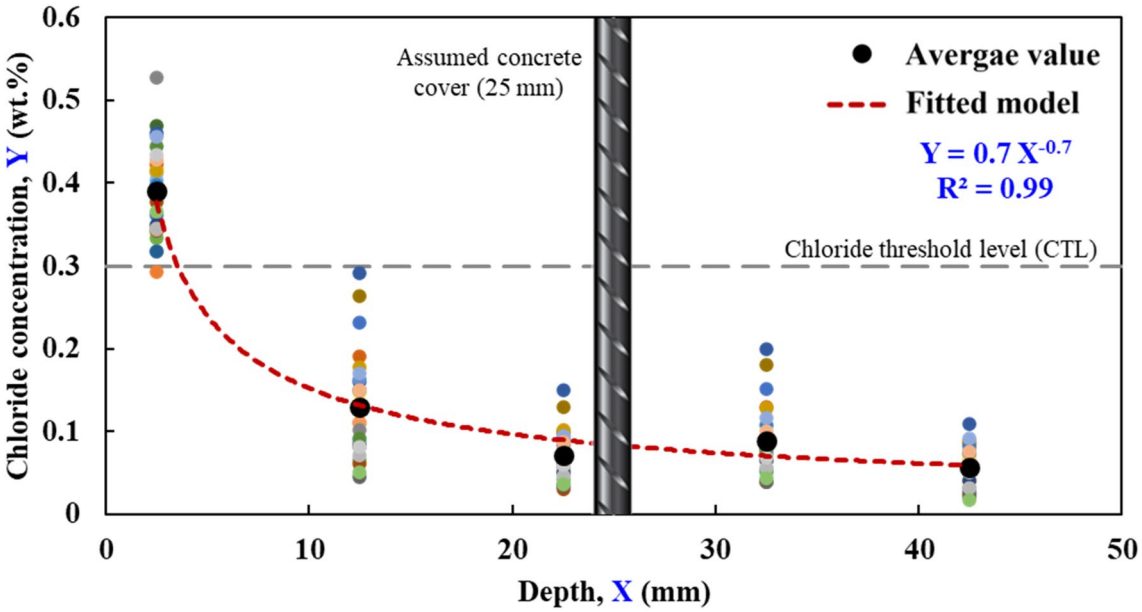

Fig. 10 Fitted model of the chloride concentration at various depths

3.5 Corrosion Current Density

The corrosion density evolution of all UHPFRC mixtures is depicted in Fig. 11. The I_{corr} values ranged from 0.005 to 0.301 μA/cm^2 (0.065–3.913 μm/year). The trend of the results showed that they fluctuated with the exposure period; however, they were less than the threshold of 0.3 μA/cm^2 (3.9 μm/year) for the initiation of active corrosion of reinforcing steel. The mixture prepared with a w/b of 0.2 and admixed with 15% SF (UHPFRC-19) showed a slightly higher I_{corr} value (0.301 μA/cm^2) than others, owing to its low OPC content (1000 kg/m^3) and higher w/b ratio (0.2). From the data plotted in Fig. 11, it can be seen that the fluctuations of the I_{corr} values tend to be nearly stabilized after 300–400 days, indicating the excellent corrosion performance of the UHPFRC mixtures after almost one year of exposure to corrosive environments (Valcuende et al., 2021). After 450 days of chloride exposure, the I_{corr} values were found to be below 0.1 μA/cm^2, implying the corrosion is in a passive state. Such a low corrosion rate has been also reported in the literature (Fan et al., 2019; Wei et al., 2022). Furthermore, it seems that the effects of the studied variables (i.e., w/b

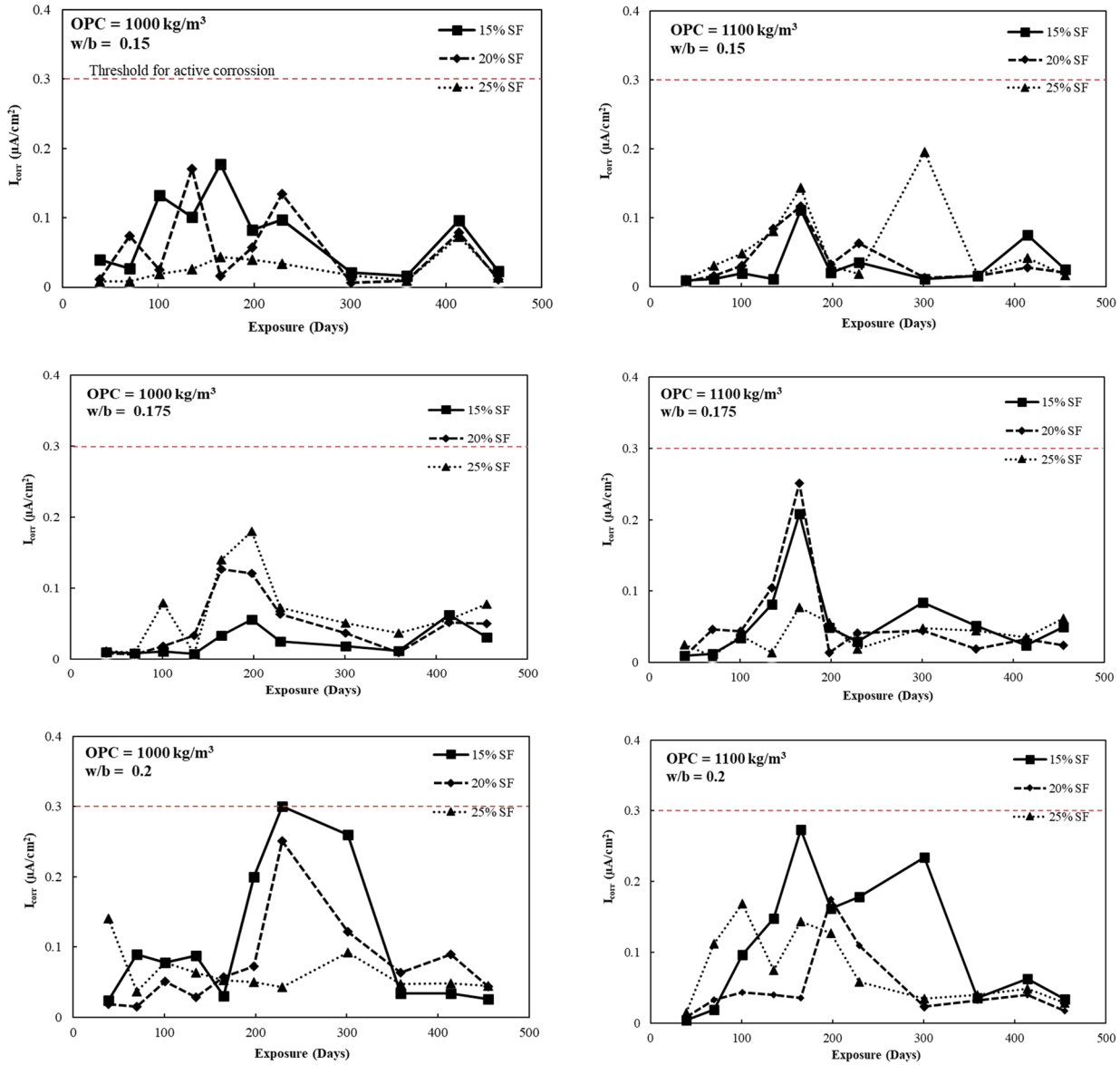

(a) OPC content of 1000 kg/m^3 at varying w/b ratios and SF dosages

(b) OPC content of 1100 kg/m^3 at varying w/b ratios and SF dosages

Fig. 11 Corrosion current density (I_{corr}) of reinforcing steel in different UHPFRC mixtures

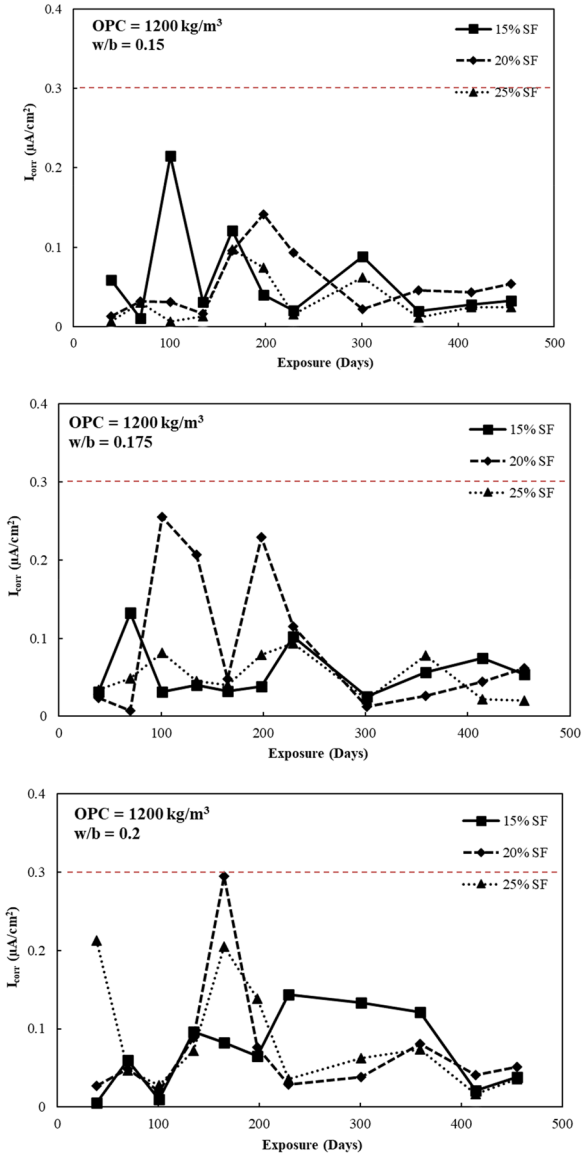

(c) OPC content of 1200 kg/m^3 at varying w/b ratios and SF dosages

Fig. 11 continued

ratio, OPC and SF contents) were negligible on the corrosion rate of the UHPFRC mixtures, suggesting corrosion is not a governed property in the selection of the optimum mixtures.

Besides the corrosion rate testing, a visual inspection of the extracted rebar was carried out. Fig. 12 displays the photographs of the extracted rebars with highlighting the portions embedded in the concrete after 450 days of exposure to chloride solution. As can be seen in these pictures, no sign of corrosion was observed. In mixture UHPFRC-19, minor corrosion spots were found, confirmed by a slightly high I_{corr} noted in this mixture, as discussed before. The visual checkup of the embedded reinforcing steel proved the admirable corrosion performance of the UHPFRC mixtures. In fact, it seems that the UHPFRC mixtures serve as a natural inhibitor against the corrosion of reinforcing steel.

In addition, pH testing was carried out using a pH meter on the samples extracted from the specimens. Fig. 13 presents the pH measurements of all mixtures. The measured pH values were in the range of 12.41–13.01, with an average value of 12.69, exceeding the limit of 10 for the initiation of reinforcing steel corrosion. These high pH values reflected the high alkalinity of the

Fig. 12 Illustration of visual inspection of embedded steel rebars in typical UHPFRC mixtures

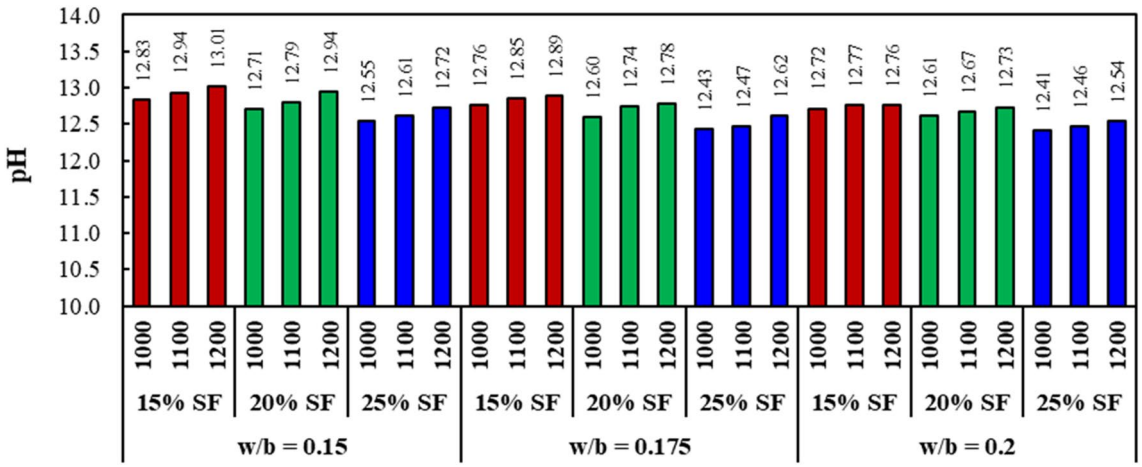

Fig. 13 The pH measurements of all UHPFRC mixtures

mixtures, which provide excellent passivity on the rebar. Therefore, it is assumed that the UHPFRC mixtures have a lower Cl^-/OH^- ratio (most probably below the limit of 0.6 for the depassivation) due to the very high pH values. This confirmed the absence of corrosion initiation risk in most of the UHPFRC mixtures.

The anticorrosion behavior of the UHPFRCs can be ascribed to several reasons, including their excellent impermeability properties, especially the resistance to chloride penetration, ultra-dense microstructure, high resistivity, and formation of the passive film around the rebar (Valcuende et al., 2021; Zheng et al., 2022).

Table 3 Summary of durability indicators of the investigated UHPFRC mixtures

Durability index	Reported range	Threshold limits	Significance
Water penetration	3.3–13.3 mm	< 30 mm	Low
Chloride ion permeability	20–242 Coulombs	< 1000 Coulombs	Very low to negligible
Electrical resistivity	26.7–78.8 kΩ cm	> 20 kΩ cm	High (likelihood of corrosion is low to negligible)
Chloride concentration	0.03–0.18 wt.%	< 0.3 wt.%	Very low (passive state)
Alkalinity	pH = 12.41–13.01	> 10	High (Passivation)
Corrosion current density	0.005–0.301 μA/cm^2	< 0.3 μA/cm^2	Low to negligible (passive state)
Visual inspection of embedded rebar	No corrosion signs	Detected corrosion rust	Corrosion of rebar does not occur

Table 4 ANOVA analysis of the factors

Source	Seq SS	Adj SS	Adj MS	*F*-value	*p*-value
Water penetration depth					
A	304.76	303.573	151.787	98.88	0.000
B	121.742	107.336	53.668	34.96	0.000
C	104.983	104.983	52.492	34.19	0.000
Chloride permeability					
A	58,016	58,016	29,008	138.25	0.000
B	27,110	27,110	13,555	64.6	0.000
C	2379	2379	1189	5.67	0.011
Electrical resistivity					
A	5700.7	5700.7	2850.3	107.25	0.000
B	1912.9	1912.9	956.5	35.99	0.000
C	1909.5	1909.5	954.7	35.92	0.000

A = w/b ratio; *B* = OPC content (kg/m^3); and *C* = SF content (%)

This was also supported by the other durability indicators as summarized in Table 3, which served as indirect assessments of the corrosion, such as very low chloride concentration (0.03–0.18 wt.%), high resistivity (26.7–78.8 kΩ cm), high alkalinity (pH = 12.41–13.01), which were much lower than the threshold limits. Thus, the corrosion of steel rebar is not a concerning issue in the UHPFRC rich-cement mixtures. This observation was also made in literature (Akeed et al., 2022; Li et al., 2020). This will be useful in prolonging the service life of important infrastructure like bridges in aggressive environments and therefore increasing the sustainability index of their construction (Dong, 2018).

3.6 Statistical Analysis and Regression Models of Transport Properties

The experimental results of the transport properties were statistically analyzed using the analysis of variance (ANOVA) method. The studied factors were the w/b ratio (denoted as A), OPC content (B), and SF content (C), which were investigated at three levels. The significance of the factors was assessed using the *F*-value and *p*-value at a 95% confidence level, i.e., the factor is considered statistically significant if its p-value is less than 0.05. Table 4 presents the results of the ANOVA analysis. The ANOVA data indicated that all key factors had a significant effect on the measured transport properties. This implied that the contributions of the mixture parameters are quite significant in the production of durable UHPFRC. In addition, the *F*-value can be used to indicate the significance degree of each factor. The w/b ratio was identified as the most influential factor on the water permeability, chloride penetrability, and electrical resistivity, while the SF content had the least significant effect.

Using the least squares method, regression models relating the factors A, B, and C with the transport properties were developed, as presented in Table 5. Fig. 14 shows the correlation between the observed values and the predicted models. A regression coefficient (R^2) of 0.90–0.99 was obtained for all the models, indicating the good accuracy of the proposed models.

Table 5 The proposed regression equations of the transport properties

Transport property	Proposed regression equation	Regression coefficient (R^2)
Water penetration depth	$WP = -3.98 + 236.62(A)^{1.5} + 1.68\times10^{67}(B)^{-22.4} + 509.93(C)^{-1.7} - 0.0817(A*B)^{0.9}$	0.96
Chloride permeability	$CP = -88.09 + 36677.51(A)^{2.8} + 1827.8(C)^{-1.4} - 2.74\times10^{-5}(A*B)^{2.9}$	0.99
Electrical resistivity	$ER = -5.27 + 5.89\times10^{-4}(A)^{-5.7} + 1.86\times10^{-8}(B)^{3} + 3.96\times10^{-4}(C)^{3.3} - 19193(A*C)^{-10.1}$	0.90

The units of WP, CP, and ER, are 'mm', 'Coulombs', and 'kΩ cm', respectively

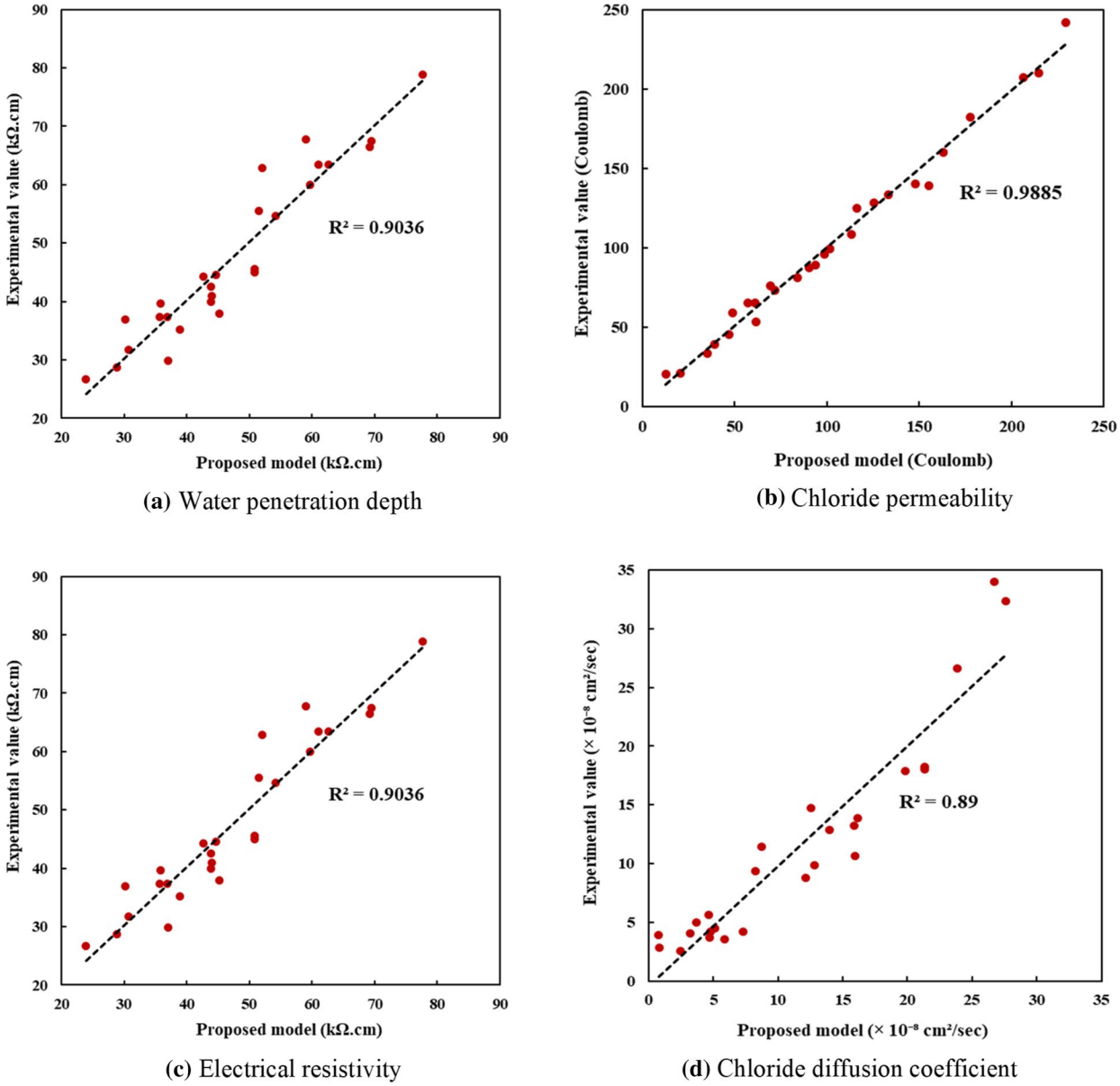

Fig. 14 Correlation between the proposed models and the measured values of the transport properties

In addition, the relationships between the studied transport properties of UHPFRC mixtures were established using the experimental data. Basically, they were related to electrical resistivity since it is an easier and quicker test. Thus, it can be used to predict other properties, including water permeability and chloride permeability. Fig. 15 shows the correlations between the transport properties. Power-curves ($Y = \alpha X^{\beta}$) were fitted on each set of data, and the corresponding regression coefficients were given. As displayed in Fig. 15a, b, a general trend was observed in which the transport properties decreased upon increasing the electrical resistivity, with slight variability at higher values of the electrical resistivity. Relating the electrical resistivity to water permeability and chloride penetrability indicated a good correlation of 0.82 and 0.89, respectively. Since electrical resistivity and chloride permeability are both electrical-based tests, they showed a higher correlation ($R^2 = 0.89$). This was also reported for normal concrete, where a strongly relation was found between the resistivity and chloride permeability (Tibbetts et al., 2020). For exploring a valid relation of the UHPFRC permeability against water and chloride, the chloride permeability was plotted against the electrical resistivity

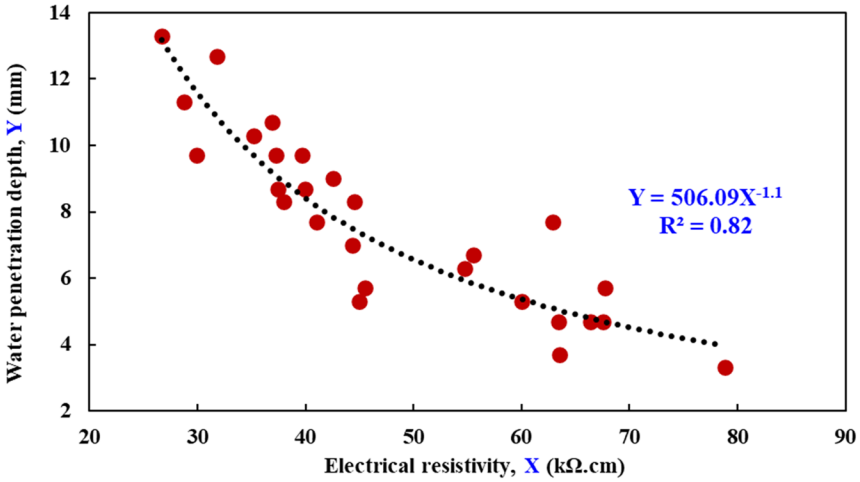

(a) Resistivity vs. Water penetration depth

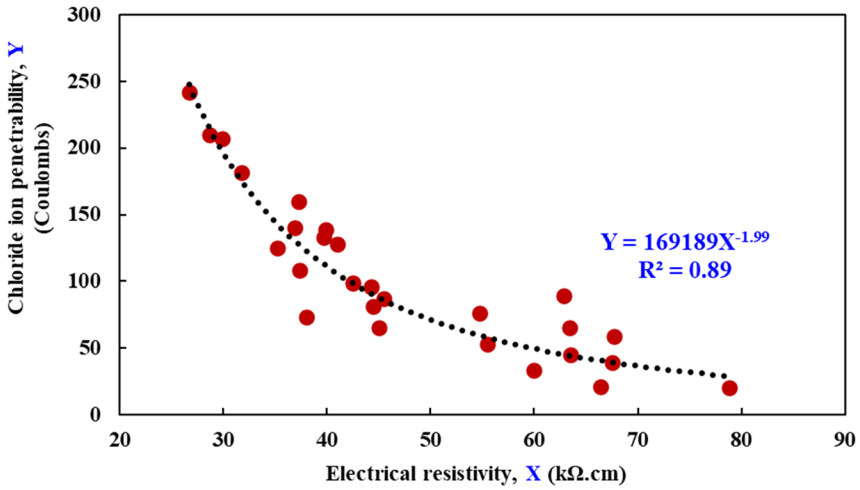

(b) Resistivity vs. Chloride permeability

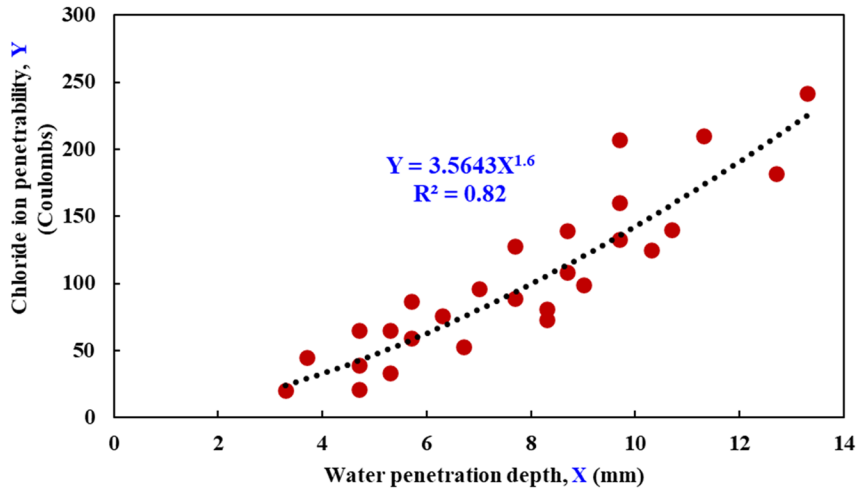

(c) Water penetration depth vs. Chloride permeability

Fig. 15 Relationships between the investigated transport properties of UHPFRC

(Fig. 15c). A good correlation was found, underlying their dependency relationship.

4 Conclusions

This research investigated the response of UHPFRC to chloride and water permeability, and model equations obtained from ANOVA and regression analysis were provided for easy data availability and design computerization purposes. In addition, a systematic investigation of the corrosion behavior of the UHPFRC mixtures was carried out. The conclusions are then drawn.

- UHPFRC had negligible water penetration (< 15 mm), negligible chloride ion permeability when the w/b ratio was 0.15 (< 100 Coulombs), and very low chloride permeability when the w/b ratio increased up to 0.2 (< 300 Coulombs). All resistivity values were greater than 20 kΩ cm (29.9–78.8 kΩ cm), while the chloride concentrations at the rebar level (0.03–0.18 wt.%) were much lower than the chloride threshold level.
- The most significant factor in controlling the transport properties of UHPFRC concrete is the w/b ratio. Silica fume and OPC contents also play a significant role in the transport and pore characteristics of UHPFRC mixtures. More significantly, the former had a higher contribution to high electrical resistivity values, while the latter influenced a greater reduction of UHPFRC's chloride ingress.
- The evolution of the corrosion density of all UHPFRC mixtures monitored over 450 days of chloride exposure demonstrated the passive state of steel rebar ($I_{corr} < 0.3$ μA/cm^2). This was also supported by the visual inspection of the extracted rebar and pH measurements. Therefore, corrosion risk is not an issue in the UHPFRC mixtures. Therefore, UHPFRC mixtures could be used successfully in an aggressive or marine environment where corrosion is of extreme challenge.
- The regression models developed could be used for durability-based design using material key parameters such as w/b ratio, SF, OPC, and surface chloride concentration (C_s) to predict the water penetration depth, chloride ion permeability, and electrical resistivity within a high correlation coefficient (R^2) of 0.90–0.99.
- The investigated correlations between the transport properties of the UHPFRC mixtures revealed that the electrical resistivity can be used as a measurement of the water penetration depth and chloride permeability.

The durability indicators imply an excellent durability performance of the UHPFRC mixtures developed in the present study. This own to the advanced mixture technology featuring high-binder content, a lower w/b ratio, and the incorporation of steel fibers. Accordingly, the service life of UHPFRC is estimated to far surpass that of conventional concrete, highlighting its effective utilization in critical infrastructure projects such as bridges. Moreover, UHPFRC presents an avenue for constructing more sustainable structures by utilizing high-strength concrete, which enables the reduction of cross-sectional dimensions of structural elements, thus minimizing material consumption.

Acknowledgements
The authors would like to thank the Department of Civil & Environmental Engineering and Interdisciplinary Research Center for Construction and Building Materials at King Fahd University of Petroleum & Minerals (KFUPM), Saudi Arabia for supporting this research.

Author contributions
SA: Conceptualization, Methodology, Formal Analysis, Writing Original Draft; AAB: Material Preparation, Investigation, Data Collection & Analysis, Writing Original Draft, Reviewing and Editing; AAF: Investigation, Formal Analysis, Validation, Reviewing and Editing; MOY: Methodology, Material Preparation, Investigation, Validation, Reviewing and Editing; MAAO: Resources, Validation, Reviewing and Editing.

Funding
None.

Data availability
Data will be made available on request.

Declarations

Competing interests
The authors declare no competing interests.

Author details
[1]Department of Civil and Environmental Engineering, King Fahd University of Petroleum & Minerals, 31261 Dhahran, Saudi Arabia. [2]Interdisciplinary Research Center for Construction and Building Materials, King Fahd University of Petroleum & Minerals, 31261 Dhahran, Saudi Arabia. [3]Department of Civil Engineering, University of Hafr Al-Batin, 31991 Hafr Al-Batin, Saudi Arabia.

Received: 28 September 2023 Accepted: 21 March 2024
Published online: 02 July 2024

References

Abbas, S., Soliman, A. M., & Nehdi, M. L. (2015). Exploring mechanical and durability properties of ultra-high performance concrete incorporating various steel fiber lengths and dosages. *Construction and Building Materials, 75*, 429–441. https://doi.org/10.1016/j.conbuildmat.2014.11.017

Abdellatief, M., Abd Elrahman, M., Elgendy, G., Bassioni, G., & Tahwia, A. M. (2023). Response surface methodology-based modelling and optimization of sustainable UHPC containing ultrafine fly ash and metakaolin. *Construction and Building Materials, 388*, 131696.

Ahmad, S. (2003). Reinforcement corrosion in concrete structures, its monitoring and service life prediction––a review. *Cement and Concrete Composites, 25*(4), 459–471. https://doi.org/10.1016/S0958-9465(02)00086-0

Ahmad, S., Al-Fakih, A., Bahraq, A. A., & Olalekan, M. (2024). Fracture toughness of UHPC mixtures:eEffects of w/b ratio, cement and silica fume contents. *Construction and Building Materials, 417*(February), 135327. https://doi.org/10.1016/j.conbuildmat.2024.135327

Ahmad, S., Bahraq, A. A., Al-Fakih, A., Maslehuddin, M., & Al-Osta, M. A. (2023). Durability and mechanical aspects of UHPC incorporating fly ash and natural pozzolan. *Arabian Journal for Science and Engineering*. https://doi.org/10.1007/s13369-023-08416-1

Ahmad, S., Hakeem, I., & Maslehuddin, M. (2016). Development of an optimum mixture of ultra-high performance concrete. *European Journal of Environmental and Civil Engineering, 20*(9), 1106–1126. https://doi.org/10.1080/19648189.2015.1090925

Ahmad, S., Zubair, A., & Maslehuddin, M. (2014). Effect of the key mixture parameters on shrinkage of reactive powder concrete. *The Scientific World Journal, 2014*, 1–8. https://doi.org/10.1155/2014/426921

Ahmad, S., Zubair, A., & Maslehuddin, M. (2015). Effect of key mixture parameters on flow and mechanical properties of reactive powder concrete. *Construction and Building Materials, 99*, 73–81. https://doi.org/10.1016/j.conbuildmat.2015.09.010

Akeed, M. H., Qaidi, S., Ahmed, H. U., Faraj, R. H., Mohammed, A. S., Emad, W., Tayeh, B. A., & Azevedo, A. R. G. (2022). Ultra-high-performance fiber-reinforced concrete. Part IV: Durability properties, cost assessment, applications, and challenges. *Case Studies in Construction Materials, 17*, e01271. https://doi.org/10.1016/j.cscm.2022.e01271

Amran, M., Huang, S.-S., Onaizi, A. M., Makul, N., Abdelgader, H. S., & Ozbakkaloglu, T. (2022). Recent trends in ultra-high performance concrete (UHPC): Current status, challenges, and future prospects. *Construction and Building Materials, 352*, 129029. https://doi.org/10.1016/j.conbuildmat.2022.129029

Angst, U., Elsener, B., Larsen, C. K., & Vennesland, Ø. (2009). Critical chloride content in reinforced concrete—a review. *Cement and Concrete Research, 39*(12), 1122–1138. https://doi.org/10.1016/j.cemconres.2009.08.006

ASTM International. (2015). *ASTM C1437: Standard test method for flow of hydraulic cement mortar* (pp. 1–2). ASTM International.

ASTM International. (2017). *ASTM C494: Standard specification for chemical admixtures for concrete*. ASTM International. https://doi.org/10.1520/C0494_C0494M-17

ASTM International. (2019a). *ASTM C1202: Standard test method for electrical indication of concrete's ability to resist chloride ion penetration* (pp. 1–8). ASTM International. https://doi.org/10.1520/C1202-19.2

ASTM International. (2019b). *ASTM C150/C150M-18: Standard specification for Portland cement*. ASTM International. https://doi.org/10.1520/C0150

ASTM International. (2021). *ASTM A820: Standard specification for steel fibers for fiber-reinforced concrete*. ASTM International.

Bahraq, A. A., Al-Osta, M. A., Ahmad, S., Al-Zahrani, M. M., Al-Dulaijan, S. O., & Rahman, M. K. (2019). Experimental and numerical investigation of shear behavior of RC beams strengthened by ultra-high performance concrete. *International Journal of Concrete Structures and Materials, 13*(6), 1–19. https://doi.org/10.1186/s40069-018-0330-z

Bajaber, M. A., & Hakeem, I. Y. (2021). UHPC evolution, development, and utilization in construction: A review. *Journal of Materials Research and Technology, 10*, 1058–1074. https://doi.org/10.1016/j.jmrt.2020.12.051

Broomfield, J. P. (2003). *Corrosion of steel in concrete: Understanding*. Spoon Press.

Bungey, J. H., & Grantham, M. G. (2006). *Testing of concrete in structures*. CRC Press.

Chen, X., Wan, D. W., Jin, L. Z., Qian, K., & Fu, F. (2019). Experimental studies and microstructure analysis for ultra high-performance reactive powder concrete. *Construction and Building Materials*. https://doi.org/10.1016/j.conbuildmat.2019.116924

Dehghanpour, H., & Yilmaz, K. (2020). The relationship between resistances measured by two-probe, Wenner probe and C1760–12 ASTM methods in electrically conductive concretes. *SN Applied Sciences, 2*, 1–10.

Dong, E., Yu, R., Fan, D., Chen, Z., & Ma, X. (2022). Absorption-desorption process of internal curing water in ultra-high performance concrete (UHPC) incorporating pumice: From relaxation theory to dynamic migration model. *Cement and Concrete Composites, 133*, 104659. https://doi.org/10.1016/j.cemconcomp.2022.104659

Dong, Y. (2018). Performance assessment and design of ultra-high performance concrete (UHPC) structures incorporating life-cycle cost and environmental impacts. *Construction and Building Materials, 167*, 414–425. https://doi.org/10.1016/j.conbuildmat.2018.02.037

Du, J., Meng, W., Khayat, K. H., Bao, Y., Guo, P., Lyu, Z., Abu-obeidah, A., Nassif, H., & Wang, H. (2021). New development of ultra-high-performance concrete (UHPC). *Composites Part B: Engineering, 224*, 109220. https://doi.org/10.1016/j.compositesb.2021.109220

El-Dieb, A. S. (2009). Mechanical, durability and microstructural characteristics of ultra-high-strength self-compacting concrete incorporating steel fibers. *Materials & Design, 30*(10), 4286–4292.

Fan, L., Meng, W., Teng, L., & Khayat, K. H. (2019). Effect of steel fibers with galvanized coatings on corrosion of steel bars embedded in UHPC. *Composites Part B: Engineering, 177*, 107445. https://doi.org/10.1016/j.compositesb.2019.107445

German Institute for Standardization. (1991). *DIN 1048: Testing of hardened concrete*. German Institute for Standardization.

Graybeal, B. A., & Hartmann, J. L. (2003). Strength and durability of ultra-high performance concrete. *Concrete bridge conference* (p. 20). Portland Cement Association.

Lambert, P., Page, C. L., & Vassie, P. R. W. (1991). Investigations of reinforcement corrosion. 2. Electrochemical monitoring of steel in chloride-contaminated concrete. *Materials and Structures, 24*(5), 351–358. https://doi.org/10.1007/BF02472068

Li, J., Wu, Z., Shi, C., Yuan, Q., & Zhang, Z. (2020). Durability of ultra-high performance concrete–A review. *Construction and Building Materials, 255*, 119296.

Lv, L.-S., Wang, J.-Y., Xiao, R.-C., Fang, M.-S., & Tan, Y. (2021). Chloride ion transport properties in microcracked ultra-high performance concrete in the marine environment. *Construction and Building Materials, 291*, 123310. https://doi.org/10.1016/j.conbuildmat.2021.123310

American Association of States Highway and Transportation Officials. (1989). *AASHTO T-277: Rapid determination of chloride permeability of concrete, Standard Specification for Transportation Materials and Methods of Sampling and Testing, Part 2: Test Methods*.

Osta, M. A., Al Khan, M. I., Bahraq, A. A., & Xu, S. Y. (2020). Application of ultra-high performance fiber reinforced concrete for retrofitting the damaged exterior reinforced concrete beam-column joints. *Earthquakes and Structures, 19*(5), 361–377. https://doi.org/10.12989/eas.2020.19.5.361

Richard, P., & Cheyrezy, M. H. (1994). Reactive powder concretes with high ductility and 200–800 MPa compressive strength. *Special Publication, 144*, 507–518.

Richard, P., & Cheyrezy, M. (1995). Composition of reactive powder concretes. *Cement and Concrete Research, 25*(7), 1501–1511.

Roux, N., Andrade, C., & Sanjuan, M. A. (1996). Experimental study of durability of reactive powder concretes. *Journal of Materials in Civil Engineering, 8*(1), 1–6.

Saleh, S., Mahmood, A. H., Hamed, E., & Zhao, X.-L. (2023). The mechanical, transport and chloride binding characteristics of ultra-high-performance concrete utilising seawater, sea sand and SCMs. *Construction and Building Materials, 372*, 130815. https://doi.org/10.1016/j.conbuildmat.2023.130815

Shi, C., Wu, Z., Xiao, J., Wang, D., Huang, Z., & Fang, Z. (2015). A review on ultra high performance concrete: Part I. Raw materials and mixture design. *Construction and Building Materials, 101*, 741–751. https://doi.org/10.1016/j.conbuildmat.2015.10.088

Soliman, N. A., & Tagnit-Hamou, A. (2017). Using particle packing and statistical approach to optimize eco-efficient ultra-high-performance concrete. *ACI Materials Journal*. https://doi.org/10.14359/51701001

Stern, M., & Geary, A. L. (1957). Electrochemical polarization I. A theoretical analysis of the shape of polarization curves. *Journal of the Electrochemical Society, 104*(1), 56–63.

Tam, C. M., Tam, V. W. Y., & Ng, K. M. (2012). Assessing drying shrinkage and water permeability of reactive powder concrete produced in Hong Kong. *Construction and Building Materials, 26*(1), 79–89. https://doi.org/10.1016/j.conbuildmat.2011.05.006

Tayeh, B. A., Aadi, A. S., Hilal, N. N., Bakar, B. H., Al-Tayeb, M. M., & Mansour, W. N. (2019). Properties of ultra-high-performance fiber-reinforced concrete (UHPFRC)—a review paper. *AIP conference proceedings*, *2157*(1).

Tibbetts, C. M., Paris, J. M., Ferraro, C. C., Riding, K. A., & Townsend, T. G. (2020). Relating water permeability to electrical resistivity and chloride penetrability of concrete containing different supplementary cementitious materials. *Cement and Concrete Composites, 107*, 103491. https://doi.org/10.1016/j.cemconcomp.2019.103491

Toledo Filho, R. D., Koenders, E. A. B., Formagini, S., & Fairbairn, E. M. R. (2012). Performance assessment of ultra high performance fiber reinforced

cementitious composites in view of sustainability. *Materials and Design, 36*, 880–888. https://doi.org/10.1016/j.matdes.2011.09.022
Valcuende, M., Lliso-Ferrando, J. R., Ramón-Zamora, J. E., & Soto, J. (2021). Corrosion resistance of ultra-high performance fibre-reinforced concrete. *Construction and Building Materials, 306*, 124914. https://doi.org/10.1016/j.conbuildmat.2021.124914
Wang, S., Wang, B., Zhu, H., Chen, G., Li, Z., Yang, L., Zhang, Y., & Zhou, X. (2023). Ultra-high performance concrete: Mix design, raw materials and curing regimes-A review. *Materials Today Communications, 35*, 105468. https://doi.org/10.1016/j.mtcomm.2023.105468
Wang, X., Wu, D., Zhang, J., Yu, R., Hou, D., & Shui, Z. (2021). Design of sustainable ultra-high performance concrete: A review. *Construction and Building Materials, 307*, 124643. https://doi.org/10.1016/j.conbuildmat.2021.124643
Wei, J., Chen, R., Huang, W., Bian, X., & Chen, B. (2022). Effect of endogenous chloride ion content and mineral admixtures on the passivation behavior of reinforcement embedded in sea-sand ultra-high performance concrete matrix. *Construction and Building Materials, 321*, 126402. https://doi.org/10.1016/j.conbuildmat.2022.126402
Wen, C., Zhang, P., Wang, J., & Hu, S. (2022). Influence of fibers on the mechanical properties and durability of ultra-high-performance concrete: A review. *Journal of Building Engineering, 52*, 104370. https://doi.org/10.1016/j.jobe.2022.104370
Yoo, D.-Y., & Yoon, Y.-S. (2016). A review on structural behavior, design, and application of ultra-high-performance fiber-reinforced concrete. *International Journal of Concrete Structures and Materials, 10*(2), 125–142. https://doi.org/10.1007/s40069-016-0143-x
Zhao, H., Hu, Y., Tang, Z., Wang, K., Li, Y., & Li, W. (2022). Deterioration of concrete under coupled aggressive actions associated with load, temperature and chemical attacks: A comprehensive review. *Construction and Building Materials, 322*, 126466. https://doi.org/10.1016/j.conbuildmat.2022.126466
Zhao, X., Lu, J.-X., Tian, W., Li, S., Qi, X., Shui, Z., & Poon, C. S. (2023). Natural bentonite as an internal curing agent in the production of eco-friendly ultra-high performance concrete with low autogenous shrinkage. *Journal of Cleaner Production, 428*, 139471. https://doi.org/10.1016/j.jclepro.2023.139471
Zheng, H., Lu, J., Shen, P., Sun, L., Poon, C. S., & Li, W. (2022). Corrosion behavior of carbon steel in chloride-contaminated ultra-high-performance cement pastes. *Cement and Concrete Composites, 128*, 104443. https://doi.org/10.1016/j.cemconcomp.2022.104443

Publisher's Note

Shamsad Ahmad Professor, Department of Civil and Environmental Engineering, King Fahd University of Petroleum & Minerals (KFUPM), Dhahran 31261, Saudi Arabia.

Ashraf A. Bahraq Postdoctoral Fellow Research, Interdisciplinary Research Center for Construction and Building Materials, King Fahd University of Petroleum & Minerals (KFUPM), Dhahran 31261, Saudi Arabia.

Amin Al-Fakih Assistant Professor, Department of Civil and Environmental Engineering, King Fahd University of Petroleum & Minerals (KFUPM), Dhahran 31261, Saudi Arabia.

Moruf Olalekan Yusuf Assistant Professor, Department of Civil Engineering, College of Engineering, University of Hafr Al-Batin (UoHB), Hafr Al-Batin 31991, Saudi Arabia.

Mohammed A. Al-Osta Associate Professor, Department of Civil and Environmental Engineering, King Fahd University of Petroleum & Minerals (KFUPM), Dhahran 31261, Saudi Arabia.